RESEARCH ARTICLE | JUNE 10 2024

Achieving semi-metallic conduction in Al-rich AlGaN: Evidence of Mott transition ⊕⊘

Shubham Mondal ⑩ ; Pat Kezer ⑩ ; Ding Wang ⑩ ; Md Mehedi Hasan Tanim ⑩ ; John T. Heron ⑩ ; Zetian Mi ➡ ⑪



Appl. Phys. Lett. 124, 243502 (2024) https://doi.org/10.1063/5.0210143









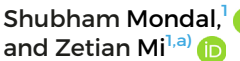
Achieving semi-metallic conduction in Al-rich AlGaN: Evidence of Mott transition @

Cite as: Appl. Phys. Lett. 124, 243502 (2024); doi: 10.1063/5.0210143 Submitted: 25 March 2024 · Accepted: 24 May 2024 · Published Online: 10 June 2024



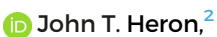














AFFILIATIONS

Department of Electrical Engineering and Computer Science, University of Michigan, Ann Arbor, Michigan 48109, USA

ABSTRACT

The development of high performance wide-bandgap AlGaN channel transistors with high current densities and reduced Ohmic losses necessitates extremely highly doped, high Al content AlGaN epilayers for regrown source/drain contact regions. In this work, we demonstrate the achievement of semi-metallic conductivity in silicon (Si) doped N-polar Al_{0.6}Ga_{0.4}N grown on C-face 4H-SiC substrates by molecular beam epitaxy. Under optimized conditions, the AlGaN epilayer shows smooth surface morphology and a narrow photoluminescence spectral linewidth, without the presence of any secondary peaks. A favorable growth window is identified wherein the free electron concentration reaches as high as $\sim 1.8 \times 10^{20}$ cm⁻³ as obtained from Hall measurements, with a high mobility of 34 cm²/V·s, leading to a room temperature resistivity of only 1 m Ω -cm. Temperature-dependent Hall measurements show that the electron concentration, mobility, and sheet resistance do not depend on temperature, clearly indicating dopant Mott transition to a semi-metallic state, wherein the activation energy (Ea) falls to 0 meV at this high value of Si doping for the AlGaN films. This achievement of semi-metallic conductivity in Si doped N-polar high Al content AlGaN is instrumental for advancing ultrawide bandgap electronic and optoelectronic devices.

Published under an exclusive license by AIP Publishing. https://doi.org/10.1063/5.0210143

Recent technological interest in III-nitride semiconductors has been centered around ultrawide bandgap materials, owing to the unique advantages that these materials offer: high operational voltages, stability at high temperatures, high frequency operation, and the potential to achieve high-performance optoelectronic devices in the deep ultraviolet (UV) regime. 1-5 In this context, Al_xGa_{1-x}N has positioned itself as the material of choice with its direct tunable ultrawidebandgap, large breakdown field, low intrinsic carrier concentration, and the ability to be doped both n- and p-type. 6-8 It is well known that in degenerately doped semiconductors, the Mott transition takes place beyond a certain value of doping, wherein electrons directly hop between orbital states located at adjacent dopant sites. Such a transition to semi-metallic conductivity has been commonly observed in semiconductors like Si, GaAs, and GaN. 10-12 However, attaining such high levels of doping to facilitate ultralow resistivity high Al content AlGaN is a significant challenge. 13 AlGaN with Al content > 0.6 may exhibit a resistivity as high as $10^5 \Omega$ cm. ¹⁴ Silicon (Si) is the commonly used n-type dopant for III-N materials, functioning as a substitutional shallow donor at the group-III site. 6,15 In high aluminum content AlGaN, the challenge in doping arises from a combination of several

factors. The activation energy increases significantly, rising from approximately 15 meV in GaN to >100 meV in AlN. Additionally, Si exhibits self-compensation behavior at elevated doping levels in high aluminum content AlGaN, resulting in decreased electron concentration and increased resistivity.¹⁷ Furthermore, the mobility in AlGaN is constrained by alloy scattering, a limitation not observed in GaN. These problems are further exacerbated in the N-polar AlGaN, as the growth on commonly used substrates like sapphire and silicon is plagued with the presence of very high density of dislocations, due to the large lattice mismatch, the formation of inversion domains, and poor surface morphology.¹⁸ In contrast, bulk AlN substrates are in the early stages of development and come with exceptionally high costs, rendering the scalability of such a growth mode impractical. As the properties of spontaneous and piezoelectric polarization are leveraged to facilitate the creation of high Al content AlGaN channel High Electron Mobility Transistors (HEMTs), a significant challenge lies in optimizing the selective regrowth of heavily doped AlGaN sourcedrain Ohmic contacts to attain high current density and avoid Ohmic heating, particularly when employing a higher Al mole fraction in the channel.2

²Department of Materials Science and Engineering, University of Michigan, Ann Arbor, Michigan 48109, USA

a) Author to whom correspondence should be addressed: ztmi@umich.edu

Recently, 4H-silicon carbide (SiC) substrate with a C-face orientation has emerged as a well-suited substrate for the epitaxy of N-polar AlN and AlGaN. In one of our recent works, we demonstrated tunable Al content N-polar AlGaN on 4H-SiC substrates with Si doping spanning orders in magnitude. The lowest recorded resistivity for high Al content was about 9 m Ω ·cm in our previous report. Recently, AlGaN films with a resistivity of 3–4 m Ω ·cm has been obtained by metalorganic chemical vapor deposition grown AlGaN films. There is a need to further reduce the resistivity for Al-rich AlGaN, for example, to achieve regrown contact access layers in AlGaN channel HEMTs with sufficiently high conductivity.

In this work, we report the attainment of semi-metallic conductivity in Si-doped N-polar AlGaN grown epitaxially on C-face 4H-SiC substrates with high Al content (~60%). By precisely controlling the growth temperature and the III/V ratio, we identify a growth window, wherein a highly conductive AlGaN epilayer is obtained with atomically smooth surface morphology. The optimized conditions for AlGaN epilayers lead to a notable reduction in defect peaks and a simultaneous enhancement in the band edge emission intensity. Hall measurements in the standard Van der Pauw configuration reveal the highest measured electron concentration of $\sim 1.8 \times 10^{20} \, \mathrm{cm}^{-3}$, with a high mobility of 34 cm²/V·s, leading to a room temperature resistivity of only $1\,\mathrm{m}\Omega$ -cm, which is the lowest reported resistivity in Al_{0.6}Ga_{0.4}N to our knowledge. Furthermore, temperature dependent Hall measurements were performed to elucidate the charge carrier transport characteristics in these films, wherein a clear signature of Mott conduction is observed for these highly conductive samples, with the vanishing of the dopant activation energy.

A Veeco GENxplor Molecular Beam Epitaxy (MBE) system was used for the epitaxy of these N-polar films, equipped with a radio frequency (RF) nitrogen plasma source (with a purity of 99.9999%) and Knudsen effusion cells for Ga (99.99999% purity), Al (99.99995% purity), and Si (99.9999%). Before introducing the C-face 4H-SiC substrate into the MBE chamber, a standard solvent cleaning process was performed with acetone, isopropyl alcohol, and deionized water. Subsequently, the substrates were baked and outgassed at 200 and 600 °C in the MBE load-lock and preparation chamber, respectively. The Si-doped AlGaN epilayer being investigated in this study is 200 nm thick and grown on top of a 200 nm AlN buffer layer [shown in Fig. 1(a)]. For Si doping of high Al content AlGaN, the challenges in attaining a satisfactory level of doping may arise significantly from

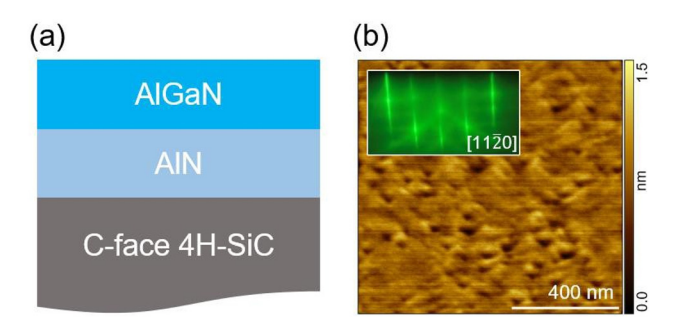


FIG. 1. (a) Schematic representation of the epitaxially grown 200 nm AlGaN heterostructure on AlN/SiC. (b) AFM image of the AlGaN epilayer (*inset*: streaky RHEED pattern observed *in-situ* after the growth of AlGaN). The r.m.s. roughness was extracted to be 0.25 nm for a 1 $\mu m \times 1 \mu m$ scanning area.

residual oxygen impurities. This is not only due to their involvement in the deep donor levels (DX) transition but also because, when combined with a high concentration of dislocations, oxygen can boost the formation of cation vacancies, serving as compensation centers.²⁵ AlN, having a lattice mismatch of lower than 1% with the underlying SiC substrate, not only produces an epitaxially smooth growth front for the subsequent growth of AlGaN but also minimizes the incorporation of O impurities from the substrate in the epilayer, which eventually helps in attaining highly conductive Si doped AlGaN epilayers.²⁶ The growth conditions of the AlN epilayer has been discussed in one of our recent works.²⁷ In this work, a favorable growth window for highly conductive Si doped AlGaN epilayers has been obtained by investigating two important epitaxy parameters, growth temperature and the N₂ flow.

Typically, a higher growth temperature results in a smooth surface morphology, consistent with our prior report. On the other hand, the surface morphology deteriorates at lower growth temperatures owing to the low adatom mobility of a N-polar surface. 6,18 However, a lower growth temperature results in fewer Al vacancies and Si-complexes, which would prove advantageous for enhancing Si doping efficiency in AlGaN films, as elaborated upon later.²⁸ In this work, by tuning the N₂ flow rate, a smooth surface morphology was achieved at a reduced growth temperature of \sim 680 °C, measured from the pyrometer reading. A higher growth rate as obtained by increasing the N2 flow also helps in reducing the resistivity of Si doped AlGaN films, as has been recently reported.²⁹ Figure 1(b) shows the AFM image of the AlGaN epilayer, wherein the r.m.s. roughness was extracted to be 0.25 nm for a $1 \, \mu m \times 1 \mu m$ scanning area. The in situ RHEED observed during the epitaxy of AlGaN is narrow and streaky, indicative of a smooth surface morphology. Furthermore, the Npolar orientation of the epitaxially grown AlGaN films was confirmed by wet-etching, as has been discussed in our previous studies.⁶

Obtaining a high conductivity in AlGaN with a substantial Al content poses a formidable challenge. The activation energy not only increases significantly but also is susceptible to high dislocation densities and compensation arising from acceptor-like defects, particularly Al vacancies. Room temperature photoluminescence experiments were carried out to investigate the effects of growth parameters in suppressing these defect states in the epitaxially grown AlGaN films. Excitation of the samples was carried out using a 193 nm ArF excimer laser, and the photoluminescence emission was gathered and examined using a Horiba iHR550 spectrometer equipped with a UV-sensitive Symphony II CCD detector.

Table I summarizes the growth conditions (growth temperature and N_2 flow) of the AlGaN samples being analyzed using photoluminescence spectroscopy.

TABLE I. Key growth parameters of samples being investigated in the present work.

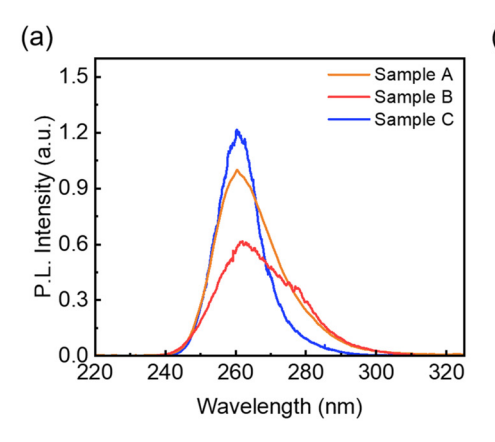
			Flux (mbar)	
Sample	Growth T (°C)	N ₂ flow (sccm)	Al	Ga
A	750	0.3	4.5×10^{-8}	5.3×10^{-7}
В	680	0.3		
C	680	0.6	5.3×10^{-8}	9.8×10^{-8}
D	680	0.65		
Е	680	0.75		

Figure 2(a) shows the comparison of room temperature PL characteristics of three samples A, B, and C, wherein sample A was grown under a metal rich regime (0.3 sccm N₂ flow) at a relatively higher temperature, with similar conditions as reported in our previous work. For sample B, the N₂ flow was kept the same; however the growth temperature was reduced, and sample C was grown at similar growth temperature as sample B but with a higher N_2 flow ~ 0.6 sccm. It can be clearly seen that the spectral linewidth of sample A is 2.3 times larger than sample C, which exhibits a narrow linewidth of only 200 meV. This asymmetric linewidth broadening toward the lower energy side can be attributed to the formation of Ga-rich clusters in samples A and B, which has been commonly observed in the growth of AlGaN under M-rich conditions.³⁰ The linewidth broadening further increases in sample B, owing to increased Ga-clusters at a lower growth T under the M-rich regime. However, increasing the N2 flow at the lower growth temperature, as in sample C, leads to a reduction of Ga-cluster formation, as is evidenced by the decreasing PL linewidth. The variations in alloy composition were linked to the reduced mobility of Al atoms due to the stronger Al-N bond in AlGaN, leading to Ga-rich inter-domain regions.³¹ Thus, by minimizing such clusters, a high spectral purity is obtained for the epitaxially grown films.

Figure 2(b) shows a comparison of room temperature PL characteristics of three samples (samples C, D, and E) grown using an increasing N₂ flow. It can be observed that for an increased N₂ flow beyond 0.6 sccm, as in sample D and sample E, a distinct secondary peak (P2) of ~280 nm is observed apart from the band edge transition peak at 260 nm (P₁). This may be attributable to the formation of Al vacancy as has been commonly observed for high Al content AlGaN samples grown under N-rich growth conditions, however, this warrants further investigation to determine the exact nature of this peak.^{29,32} Upon fitting the PL data, it is found that the integrated intensity ratio (P1/P2) is 77 for sample C, implying that such a defect related emission is hardly noticeable. However, for sample D, it is 1.51, and for sample E, it further drops to 0.86. Furthermore, the overall integrated intensity of the band edge photoluminescence emission is 20 times higher for sample C compared with sample E. A significantly high radiative recombination rate is achieved, thus implying the reduction of significant defects or dislocations in the epitaxially grown AlGaN films under optimized conditions. This indicates that the band edge peak starts to dominate as we reduce the N₂ flow rate. However, a sufficiently high N2 flow is required to minimize the formation of Ga-rich clusters as has been previously observed in photoluminescence studies of high Al content (x > 0.5) AlGaN films.³⁰

Reducing Al vacancies is known to directly impact the doping concentration of the films. Studies indicate that a decrease in group III-vacancies leads to reduced self-compensation in highly silicondoped AlGaN epilayers. To analyze the impact of growth conditions on the Si doping limits of the samples, two sets of growth conditions were considered: Condition A: high metal flux and low N_2 flow (similar to sample A) and Condition B: low metal flux and relatively high N_2 flow (similar to sample C), as described in Table I. Six samples were grown for each of these two conditions (A1, ..., A6) and (C1, ..., C6), with the Si cell temperatures varied from $1200\,^{\circ}$ C to $1360\,^{\circ}$ C. Ti ($10\,\text{nm}$)/Au ($100\,\text{nm}$) electrodes were patterned by photolithography in the standard van der Pauw configuration, and Hall measurements were carried out to determine the carrier concentration, mobility, and resistivity of the AlGaN epilayers in each of these samples.

As can be seen in Fig. 3(a), the carrier concentration steadily increases as we increase the Si cell temperature, indicating proportionate carrier incorporation and activation in the AlGaN film. Even though a similar carrier concentration is achieved for a Si cell temperature of 1200 °C for both the growth conditions, the rate of increase in carrier concentration with increasing Si cell temperature is much more pronounced in Condition B compared to Condition A. The highest electron concentration is $\sim 1.8 \times 10^{20} \, \text{cm}^{-3}$ in Condition B, indicating highly efficient doping incorporation and activation in the optimized epitaxial conditions. On the high doping side, the formation of metal vacancy-related point defects along with the growth temperature determines the limit for the maximum achievable carrier concentration. In our optimized growth conditions, suppressing such metal vacancies is achieved as discussed in Figs. 2(a) and 2(b), and the growth temperature is lower than in Condition A, thus avoiding the self-compensation of Si by the formation of DX centers, as has been observed in previous studies.^{23,29} However, when upon exceeding the upper doping limit with silicon (Si), the surplus Si incorporated creates an acceptor state, compensating for the remaining Si donors. This emphasizes the crucial role of self-compensation at higher Si levels, ultimately defining the upper doping limit for silicon in this context. As a result, heavily Sidoped AlGaN demonstrates elevated resistivity attributed to a substantial decrease in electron concentration. 33,34 A similar "knee-behavior" is clearly observed for our samples at a Si cell temperature of ~1330 °C, above which the carrier concentration drops sharply for both groups of samples. This drop in carrier concentration is primarily attributed to the formation of V_{III}-nSi_{III} complexes at elevated Si doping levels. Figure 3(b) shows the mobility of samples in the two growth



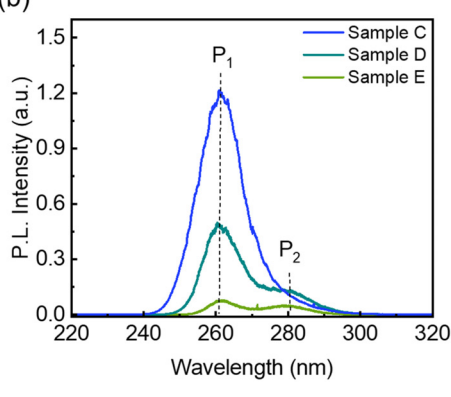


FIG. 2. Photoluminescence spectroscopy results showing the room-temperature emission for (a) samples A, B, and C, with the band edge transition peak at 260 nm (P₁) and a clear asymmetric broadening observed for samples A and B. (b) Photoluminescence spectra of samples C, D and E showing the presence of a distinct secondary peak P₂ $\sim\!280\,\mathrm{nm}$ for samples D and E.

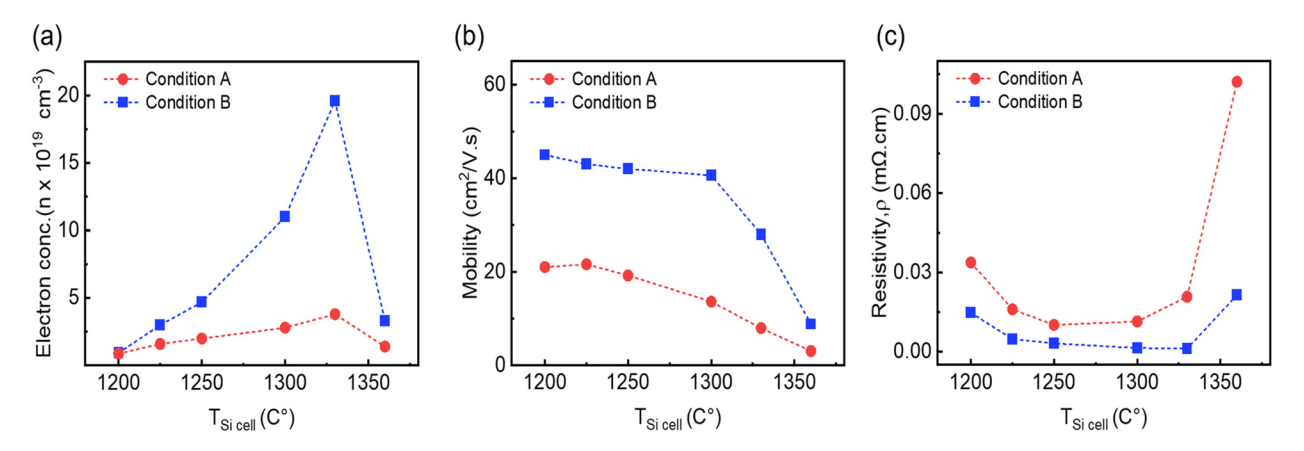


FIG. 3. Comparative analysis of (a) electron concentration, (b) mobility, and (c) resistivity of AlGaN epilayers grown under Condition A and Condition B as a function of Si cell temperature. (Note: Six samples were grown for each of these two conditions (A1, ..., A6) and (C1, ..., C6), with the Si cell temperatures varied from 1200 to 1360 °C).

conditions as a function of Si cell temperature. The highest recorded value of mobility for Condition B is 45 cm²/V·s at a corresponding electron concentration of 2×10^{19} cm⁻³, whereas for Condition A, it is only $\sim 20 \text{ cm}^2/\text{V} \cdot \text{s}$. Even for the highest recorded electron concentration of $1.8 \times 10^{20} \, \text{cm}^{-3}$, the mobility is sustained at $34 \, \text{cm}^2/\text{V} \cdot \text{s}$. Carbon has been identified as a species with a negative charge state (C_N) in n-type III-Ns that can act as a compensator and often result in a mobility collapse. 28,35 The optimized growth conditions with a higher N₂ flow has been effective in suppressing the incorporation of C_N in AlGaN epilayers, thus resulting in enhanced mobility values. As seen in the plot of resistivity as a function of Si cell temperature in Fig. 3(c), the lowest recorded room temperature resistivity value is 1 m Ω ·cm. This value is \sim 3 times lower than the lowest reported resistivity in similar Al content AlGaN reported to date. The lowest resistivity was recorded for Si cell temperature of ~1330 °C, beyond which the resistivity increases sharply, consistent with the observed "knee-behavior" in the electron concentration. Moreover, dislocations play a critical role in determining the resistivity of a sample, with an equivalent acceptor concentration equal to their density.³⁶ The growth of N-polar AlGaN with an AlN buffer on SiC offers <1% lattice mismatch, resulting in highly reduced dislocation densities. Moreover, the observed low variation in carrier concentration (n) and resistivity (ρ) originates from the semi-metallic state owing to the high doping concentration used in this study. In our previous study on the Si doping of N-polar AlGaN, a similar heterostructure was utilized, and we observed significant yet controllable variation in carrier concentration (n) and resistivity (ρ) . However, it is noteworthy that the doping concentration employed in that study was not as high as that used in the present investigation. There exists an AlN/AlGaN interface within the heterostructure that could potentially influence the depicted charge transport characteristics in this manuscript.³⁷ Given that the carrier concentration obtained in this study is substantially higher than that in our previous research, it can be deduced that the interface plays a less significant role in modulating the charge transport properties.

To gain further insight into the carrier transport mechanism of the lowest resistivity high Al content AlGaN epilayers obtained in this film (Condition B, $T_{Si\ cell}=1330\,^{\circ}$ C), temperature-dependent Hall effect measurements were performed in a Quantum Design physical property

measurement system (PPMS), and the sample was configured in the standard van der Pauw geometry. The sample was held at each temperature for 30 min prior to measurement to allow for adequate environmental equilibration, starting at 10 K. The temperature was increased at a rate of 5 K/min between measurements. Sheet resistance and Hall effect measurements were performed using a Keithley 2450 to source and sense the signals and Keithley 3706A-S to switch between the various van der Pauw configurations. The source current ranged between $100\,\mu\text{A}$ and $1\,\text{mA}$ for each sample. The magnetic field was swept from $+0.32\,\text{T}$ to $-0.32\,\text{T}$ in increments of $2\,\text{mT}$ for the Hall effect measurements.

At high Si doping levels, transition to a metallic state is observed for AlGaN films, wherein the activation energy (E_a) falls to ~ 0 meV. As the conduction does not rely on thermal activation of electrons, the conductivity remains relatively independent of temperature. The incorporation of Si is almost similar to the measured electron concentration, owing to Mott transition induced semi-metallic conductivity state, as has been reported in some previous studies. 15 From the Arrhenius plot in Fig. 4(a), the carrier concentration is constant at $\sim 1.8 \times 10^{20} \,\mathrm{cm}^{-3}$, i.e., the slope (E_a) is found to be 0 meV, thus indicating a clear transition to the metallic state. Moreover, at high doping levels, as the Mott conduction dominates, it strongly reduces the temperature dependence of transport, so mobility stays relatively constant. A similar trend has been observed for our films, with the mobility being constant at 34 cm²/V·s, throughout the temperature range, as seen in Fig. 4(b). Figure 4(c) shows the sheet resistance of the AlGaN film to be exceptionally low at \sim 48 Ω /sq.

Moreover, the sheet resistance does not increase with decrease in temperature, as is generally expected for moderately doped AlGaN films. Finally, we present a benchmarking of the free electron concentration and resistivity of the AlGaN films with some other reports in literature, as shown in Fig. 4(d). $^{6.15,28,33,36,38-42}$ Note that this comparison includes Si-doped AlGaN films, either M-polar or N-polar, albeit with a similar Al content. It is evident from this study that the recorded lowest resistivity value of 1 m Ω -cm exceeds the best results documented in the literature for high Al content ($\sim\!60\%$) AlGaN to the best of our knowledge, considering both carrier concentration and resistivity.

In conclusion, we present an effective route to realize high Al content, highly conductive N-polar AlGaN films on 4H-SiC substrates.

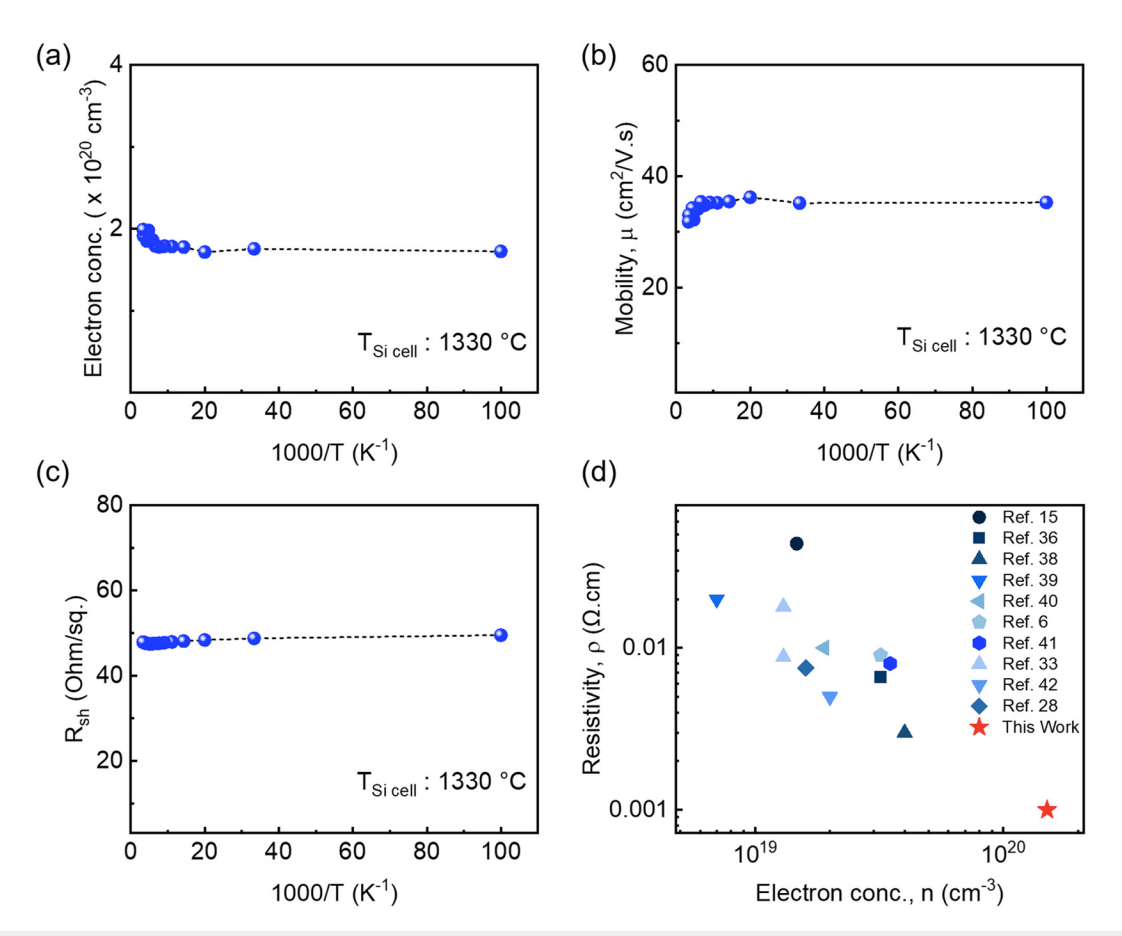


FIG. 4. Temperature dependent Hall measurements showing the independence of (a) electron concentration, (b) mobility, and (c) sheet resistance with varying temperatures for the optimized growth conditions (sample C with T_{Si cell} = 1330 °C) showing, suggesting the attainment of Mott transition induced metallic conductivity state for heavily doped AlGaN:Si films. (d) Comparison of the free electron concentration and resistivity of our Si-doped AlGaN films with some other reports in literature.

The epitaxially grown films show smooth surface morphology, and optimization of growth conditions has led to the identification of a growth window, which helps minimize the formation of both Garich clusters and Al vacancies. Owing to the highly efficient doping, Mott transition to the semi-metallic state has been achieved in this work, with an exceptionally high free electron concentration and the lowest recorded resistivity till date to the best of our knowledge. The highly conductive high Al content AlGaN epilayers can be translated to low-resistance regrown contact regions in AlGaN channel HEMTs. Therefore, this study is instrumental for the development of high-power RF and millimeter-wave HEMTs, which may also prove valuable in enhancing the breakdown voltages for power switching applications due to the ultrawide bandgap of AlGaN.

This work was supported by the U.S. Army Research Office under Grant No. W911NF2310142 and the NSF MRSEC DMR-2011839. The authors would like to thank Mingtao Hu and Professor Emmanouil Kioupakis for discussions related to this work. Portions of this work were performed at the Lurie Nanofabrication Facility, Michigan Center for Materials Characterization at the University of Michigan.

AUTHOR DECLARATIONS Conflict of Interest

Some IP related to this work has been licensed to NS Nanotech, Inc., which was co-founded by Z. Mi. The University of Michigan and Mi have a financial interest in the company.

Author Contributions

Shubham Mondal: Conceptualization (equal); Formal analysis (equal); Investigation (equal); Methodology (equal); Writing – original draft (equal). Pat Kezer: Data curation (equal); Investigation (equal); Methodology (equal). Ding Wang: Conceptualization (equal); Supervision (equal); Validation (equal). Md Mehedi Hasan Tanim: Investigation (equal). John T. Heron: Funding acquisition (equal); Supervision (equal); Writing – review & editing (equal). Zetian Mi: Conceptualization (equal); Funding acquisition (equal); Project administration (equal); Supervision (equal); Writing – review & editing (equal).

DATA AVAILABILITY

The data that support the findings of this study are available from the corresponding author upon reasonable request.

REFERENCES

- ¹O. Ambacher, J. Phys. D: Appl. Phys. **31**(20), 2653 (1998).
- ²U. K. Mishra, P. Parikh, and Y.-F. Wu, Proc. IEEE **90**(6), 1022 (2002).
- ³T. Paskova, D. A. Hanser, and K. R. Evans, Proc. IEEE **98**(7), 1324 (2010).
- ⁴Y. Wu, X. Liu, A. Pandey, P. Zhou, W. J. Dong, P. Wang, J. Min, P. Deotare, M. Kira, and E. Kioupakis, Prog. Quant. Electron. 85, 100401 (2022).
- ⁵A. Pandey and Z. Mi, IEEE J. Quant. Electron. **58**(4), 1 (2022).
- ⁶S. Mondal, D. Wang, A. F. M. Anhar Uddin Bhuiyan, M. Hu, M. Reddeppa, P. Wang, H. Zhao, and Z. Mi, Appl. Phys. Lett. **123**(18), 182106 (2023).
- ⁷D. Li, K. Jiang, X. Sun, and C. Guo, Adv. Opt. Photonics **10**(1), 43 (2018).
- ⁸B. Sarkar, S. Washiyama, M. H. Breckenridge, A. Klump, J. N. Baker, P. Reddy, J. Tweedie, S. Mita, R. Kirste, and D. L. Irving, ECS Trans. 86(12), 25 (2018).
- ⁹N. F. Mott, Can. J. Phys. **34**(12A), 1356 (1956).
- ¹⁰ A. Ajay, J. Schörmann, M. Jiménez-Rodriguez, C. B. Lim, F. Walther, M. Rohnke, I. Mouton, L. Amichi, C. Bougerol, and M. I. Den Hertog, J. Phys. D: Appl. Phys. 49(44), 445301 (2016).
- ¹¹E. Prati, M. Hori, F. Guagliardo, G. Ferrari, and T. Shinada, Nat. Nanotechnol. 7(7), 443 (2012).
- ¹²M. Benzaquen, D. Walsh, and K. Mazuruk, Phys. Rev. B **36**(9), 4748 (1987).
- ¹³R. Collazo, S. Mita, J. Xie, A. Rice, J. Tweedie, R. Dalmau, and Z. Sitar, Phys. Status Solidi c 8(7-8), 2031 (2011).
- ¹⁴J. Li, K. B. Nam, J. Y. Lin, and H. X. Jiang, Appl. Phys. Lett. **79**(20), 3245 (2001)
- 15S. Bharadwaj, S. M. Islam, K. Nomoto, V. Protasenko, A. Chaney, H. G. Xing, and D. Jena, Appl. Phys. Lett. 114(11), 113501 (2019).
- ¹⁶B. Borisov, V. Kuryatkov, Y. Kudryavtsev, R. Asomoza, S. Nikishin, D. Y. Song, M. Holtz, and H. Temkin, Appl. Phys. Lett. 87(13), 132106 (2005).
- 17J. S. Harris, J. N. Baker, B. E. Gaddy, I. Bryan, Z. Bryan, K. J. Mirrielees, P. Reddy, R. Collazo, Z. Sitar, and D. L. Irving, Appl. Phys. Lett. 112(15), 152101 (2018)
- ¹⁸P. Wang, D. Wang, S. Mondal, Y. Wu, T. Ma, and Z. Mi, ACS Appl. Mater. Int. 14(13), 15747 (2022).
- ¹⁹J. Singhal, J. Encomendero, Y. Cho, L. van Deurzen, Z. Zhang, K. Nomoto, M. Toita, H. G. Xing, and D. Jena, AIP Adv. 12(9), 095314 (2022).
- ²⁰S. Bajaj, F. Akyol, S. Krishnamoorthy, Y. Zhang, and S. Rajan, Appl. Phys. Lett. 109(13), 133508 (2016).
- ²¹I. Abid, J. Mehta, Y. Cordier, J. Derluyn, S. Degroote, H. Miyake, and F. Medidoub, Electronics 10(6), 635 (2021).
- ²²J. Lemettinen, H. Okumura, I. Kim, C. Kauppinen, T. Palacios, and S. Suihkonen, J. Cryst. Growth 487, 12 (2018).
- ²³C. J. Zollner, Y. Yao, M. Wang, F. Wu, M. Iza, J. S. Speck, S. P. DenBaars, and S. Nakamura, Crystals 11(8), 1006 (2021).

- ²⁴J. Wang, B. K. SaifAddin, C. J. Zollner, B. Bonef, A. S. Almogbel, Y. Yao, M. Iza, Y. Zhang, M. N. Fireman, and E. C. Young, Opt. Exp. 29(25), 40781 (2021).
- ²⁵ M. L. Nakarmi, K. H. Kim, K. Zhu, J. Y. Lin, and H. X. Jiang, Appl. Phys. Lett. 85(17), 3769 (2004).
- 26M. Hu, P. Wang, D. Wang, Y. Wu, S. Mondal, D. Wang, E. Ahmadi, T. Ma, and Z. Mi, APL Mater. 11(12), 121111 (2023).
- ²⁷J. Lu, J.-T. Chen, M. Dahlqvist, R. Kabouche, F. Medjdoub, J. Rosen, O. Kordina, and L. Hultman, Appl. Phys. Lett. 115(22), 221601 (2019).
- 28S. Washiyama, P. Reddy, B. Sarkar, M. H. Breckenridge, Q. Guo, P. Bagheri, A. Klump, R. Kirste, J. Tweedie, and S. Mita, J. Appl. Phys. 127(10), 105702 (2020).
- ²⁹A. S. Almogbel, C. J. Zollner, B. K. Saifaddin, M. Iza, J. Wang, Y. Yao, M. Wang, and H. Foronda, "Igor Prozheev, and Filip Tuomisto," AIP Adv. 11(9), 095119 (2021).
- ³⁰S. Zhao, S. Y. Woo, M. Bugnet, X. Liu, J. Kang, G. A. Botton, and Z. Mi, Nano Lett. 15(12), 7801 (2015).
- ³¹S. Marcinkevičius, R. Jain, M. Shatalov, J. Yang, M. Shur, and R. Gaska, Appl. Phys. Lett. **105**(24), 241108 (2014).
- ³²A. Sedhain, J. Y. Lin, and H. X. Jiang, Appl. Phys. Lett. **100**(22), 221107 (2012).
- ³³P. Reddy, Q. Guo, J. Tweedie, S. Washiyama, F. Kaess, S. Mita, M. H. Breckenridge, R. Kirste, R. Collazo, and A. Klump, Presented at the 2018 IEEE Research and Applications of Photonics in Defense Conference (RAPID) (2018).
- 34I. Bryan, Z. Bryan, S. Washiyama, P. Reddy, B. Gaddy, B. Sarkar, M. Hayden Breckenridge, Q. Guo, M. Bobea, and J. Tweedie, Appl. Phys. Lett. 112(6), 062102 (2018).
- 35F. Kaess, S. Mita, J. Xie, P. Reddy, A. Klump, L. H. Hernandez-Balderrama, S. Washiyama, A. Franke, R. Kirste, A. Hoffmann, R. Collazo, and Z. Sitar, J. Appl. Phys. 120, 105701 (2016).
- ³⁶E. C. H. Kyle, S. W. Kaun, P. G. Burke, F. Wu, Y.-R. Wu, and J. S. Speck, J. Appl. Phys. 115(19), 193702 (2014).
- ³⁷D. C. Look and R. J. Molnar, Appl. Phys. Lett. **70**, 3377 (1997).
- ³⁸K. Nagata, H. Makino, T. Yamamoto, K. Kataoka, T. Narita, and Y. Saito, Appl. Phys. Exp. **13**(2), 025504 (2020).
- ³⁹J. Pyeon, J. Kim, M. Jeon, K. Ko, E. Shin, and O. Nam, Jpn. J. Appl. Phys. 54(5), 051002 (2015).
- ⁴⁰S. Xu, X. Zhang, X. Luo, R. Fang, J. Lyu, M.-J. Lai, and G. Hu, Mater. Sci. Semicond. Process. **160**, 107447 (2023).
- ⁴¹R. France, T. Xu, P. Chen, R. Chandrasekaran, and T. D. Moustakas, Appl. Phys. Lett. **90**(6), 062115 (2007).
- ⁴²J. Yang, Y. H. Zhang, D. G. Zhao, P. Chen, Z. S. Liu, and F. Liang, J. Cryst. Growth 570, 126245 (2021).